Available online at www.sciencedirect.com
SCIENCE DIRECT®
PERGAMON
International Journal of Multiphase Flow 29 (2003) 1451–1471
International Journal of Multiphase Flow
www.elsevier.com/locate/ijmulflow

Bubble size in coalescence dominant regime of turbulent air–water flow through horizontal pipes

M. Mahbubur Razzaque [a], Artin Afacan [a], Shijie Liu [a], K. Nandakumar [a], Jacob H. Masliyah [a,*], R. Sean Sanders [b]

[a] *Department of Chemical and Materials Engineering, University of Alberta, Edmonton, Alta., Canada T6G 2G6*
[b] *Syncrude Canada Ltd., Edmonton Research Centre, 9421-17 Ave., Edmonton, AB, Canada T6N 1H4*

Received 3 June 2002; received in revised form 10 June 2003

Abstract

An experimental study was performed in a 25.4 mm ID pipeline to evaluate the development of the bubble size distribution in the horizontal flow of an air–water system. As the air stream enters into the flowing water stream through a T-injector, it breaks into bubbles with a log-normal size distribution. Because of the small water velocity (1–3 m/s) and small initial bubble size, coalescence, not breakage, plays the dominant role in the present study. The effects of average water velocity, air volume fraction and air injector diameter on the initial bubble size distribution and its evolution along the length of the pipe in the coalescence dominant regime are investigated.

At larger water velocities, the log-normal bubble size distributions are also maintained downstream of the injector. At smaller velocities, the distributions deviate slightly from the log-normal pattern. For all distributions, the value of the ratio $d_{99.8}/d_{32}$ is about 2.2 and is fairly independent of average water velocity, pipe length, air volume fraction and air injector diameter. It is found that at large velocities of water, the prediction of d_{max} through Levich's breakup theory agrees well with the experimental $d_{99.8}$ values for air volume fraction up to 0.003.

Keywords: Two-phase horizontal flow; Air–water pipe flow; Dispersed bubbly flow; Coalescence dominant regime; Bubble size distribution; Bubble breakup; Bubble coalescence

* Corresponding author. Address: Department of Chemical and Materials Engineering, 536 Chemical and Materials Engineering Bldg., University of Alberta, Edmonton, AB, Canada TG9 96. Tel.: +1-780-492-4673; fax: +1-780-492-2881.
E-mail address: jacob.masliyah@ualberta.ca (J.H. Masliyah).

0301-9322/$ - see front matter
doi:10.1016/S0301-9322(03)00123-X

1. Introduction

In mineral processing industries, effective air bubble–particle attachment and subsequent mineral flotation is critical. This process is highly dependent upon the size and surface characteristics of both the solid particles and the dispersed air phase. Generally, bubble–particle attachment occurs in a flotation cell. In the oil sands industry of northern Alberta, bitumen is recovered from oil sand. The attachment of air bubbles to bitumen droplets occurs during the turbulent flow of a concentrated slurry of oil sand and water as the slurry is transported from the mine site to the extraction facilities. Thus it is essential to have a good understanding and reasonable estimate of the effect of turbulent slurry flow on bubble size distribution to successfully design and operate a system that can achieve high bitumen recoveries.

In other applications, air is sometimes injected into hydrotransport pipelines because particle–air aggregates remain suspended under conditions at which the particles themselves would settle out of the flow.

Because of the complexity and experimental design challenges involved in studying bubble size in highly concentrated solid–liquid flows, initial studies of air–water–sand systems have been limited to low concentrations of air and sand. This paper deals with some initial experiments conducted with a two-phase air–water system. Three-phase air–water–sand experiments are currently underway and these results will be presented in a subsequent paper.

Although many theoretical and experimental studies are reported in the literature for the prediction of drop size distribution in two-phase liquid–liquid dispersions in stirred tanks (Calderbank, 1958; Shinnar, 1961; Shinnar and Church, 1960; Church and Shinnar, 1961; Calabrese et al., 1986a,b; Davies, 1987; Tsouris and Tavlarides, 1994; Liu and Li, 1999; etc.) and transport pipelines (Ward and Knudsen, 1967; Swartz and Kessler, 1970; Collins and Knudsen, 1970; Kubie and Gardner, 1977; Karabelas, 1978; Kostoglou and Karabelas, 1998; Angeli and Hewitt, 2000; Angeli, 2001; Simmons and Azzopardi, 2001; etc.), there are very few studies available for the prediction of bubble size in two-phase air–liquid flows. These studies include Walter and Blanch (1986) and Hesketh et al. (1987, 1991a,b) for turbulent air–water flow through pipelines and Parthasarathy et al. (1991) for that in stirred tanks. They performed experiments in dispersed bubble flow regime obtained at a relatively large water velocity. They used a small volume fraction of air to inhibit coalescence and measured the maximum bubble size of the stable distribution, which evolved through a breakup mechanism only. In a recent study, Andreussi et al. (1999) examined both coalescence and breakup and developed an empirical relation for the maximum stable bubble size in horizontal pipe flow. Since the primary focus of all the studies mentioned above was to define a criterion for the stability of a solitary bubble against breakup, they used specially designed coaxial large diameter air injectors in order to generate large bubbles at the inlet.

In the present experiment, an air supply line is connected to a horizontal flow loop (25.4 mm ID) through a simple T-junction. The average velocity of water, U, averaged across the pipe cross-section is less than 3 m/s, which is relatively small compared to that of other experimental studies (Hesketh et al., 1987, 1991a,b; Andreussi et al., 1999). In an industrial application, a T-junction injector is easier to install and is of more practical interest. However, with T-junction injectors, bubbles formed at the inlet are not as large as they are with coaxial injectors. Due to small water velocities and small initial bubble sizes, coalescence played a dominant role in the present experiments.

In this paper, the effects of average water velocity, air volume fraction and air injector diameter on the initial bubble size distribution and its evolution along the pipe in the coalescence dominant regime have been analyzed and the influence of these parameters on bubble size prediction using existing theories have been investigated.

2. Bubble size in turbulent pipe flow: theory

In turbulent flow of a liquid containing dispersed bubbles, breakup and coalescence usually take place continuously and these processes determine the bubble size distribution. If the residence time of the bubbles is sufficiently long (i.e., if the pipe is long), a local dynamic equilibrium between coalescence and breakup is established. Two important parameters, the maximum bubble diameter, d_{max}, and the minimum bubble diameter, d_{min}, can be identified in such conditions (Shinnar, 1961; Liu and Li, 1999). Bubbles having diameters smaller than d_{min} will have a high tendency to coalesce whereas those having diameters larger than d_{max} will have a high tendency to break up.

2.1. Maximum bubble diameter

Since the fundamental contributions by Kolmogoroff (1949) and Hinze (1955), bubble breakup in the inertial subrange of locally isotropic turbulence has been extensively studied by many, including Levich (1962), Sevik and Park (1973), Hesketh et al. (1987, 1991a,b), Wilkinson et al. (1993), Martinez-Bazan et al. (1999a,b) and Risso (2000). The general understanding is that if the diameter of a bubble is larger than the Kolmogoroff length scale,

$$\lambda = (\nu_c^3/\varepsilon)^{1/4}$$

and is of the order of the length of the energy-containing eddies in the continuous fluid, it tends to deform under the action of the fluctuating eddies. Here, ν_c and ε denote kinematic viscosity of the continuous fluid and turbulent kinetic energy dissipation rate per unit mass, respectively. The deformation sets up motion in the dispersed phase and makes the bubble unstable due to an increase in its surface energy. Levich (1962) hypothesized that a deformed bubble breaks up when the internal pressure force overcomes the surface force. Considering a force balance between these two forces, he obtained a critical Weber number,

$$We_c = \frac{\tau}{\sigma/d_{max}}\left(\frac{\rho_d}{\rho_c}\right)^{1/3} \tag{1}$$

Here, d_{max} is the diameter of the largest bubble that can resist the breakup in a turbulent flow field, σ is the interfacial tension and ρ_c and ρ_d are the continuous and dispersed phase densities, respectively and τ is the stress on the bubble surface due to the turbulent fluctuating eddies in the continuous phase. Based on this definition of the critical Weber number, Hesketh et al. (1987) derived the following equation for d_{max} in pipe flows:

$$d_{\max} = 1.38(We_c)^{0.6}\left[\frac{\sigma^{0.6}}{\rho_c^{0.5}\mu_c^{0.1}}\right]\left(\frac{\rho_c}{\rho_d}\right)^{0.2}\left(\frac{D^{0.5}}{U^{1.1}}\right) \tag{2}$$

Here, D is pipe diameter, U is average water velocity and μ_c is dynamic viscosity of the continuous phase, i.e. water. Using the data of Holmes (1973), Kubie and Gardner (1977) and Karabelas (1978), Hesketh et al. (1987) determined $We_c \approx 1.1$. These studies showed that Eq. (2) can satisfactorily predict the maximum size of both bubbles ($\rho_d \ll \rho_c$) and drops ($\rho_d \approx \rho_c$). The air–water experimental data of Andreussi et al. (1999) also confirm Eq. (2). Extrapolation of their data for low void fraction of air gives a value of critical Weber number, We_c, of 1.05 which is close to the value given by Hesketh et al. (1987).

2.2. Minimum bubble diameter

The concept of minimum bubble diameter, $d_{\min}$, has been developed from the studies of coalescence of drops and bubbles by many researchers; e.g., to name a few, Shinnar (1961), Thomas (1981), Chesters (1991), Tsouris and Tavlarides (1994) and Liu and Li (1999). Bubbles collide with each other due to the fluctuating eddies in a turbulent flow. As two colliding bubbles approach each other, a liquid film is trapped between them. For coalescence to occur this liquid film must drain out and rupture. However, before coalescence occurs, the bubbles may separate if they possess sufficiently high energy. A simple analytical solution for the minimum bubble diameter, $d_{\min}$, is available only if it is assumed that the bubble surfaces are immobilized by the presence of impurities, e.g., surfactants and particles. However, for air–water systems without any surfactants or impurities, the bubble surfaces are mobile and no explicit solution is available for $d_{\min}$. Using numerical methods, Liu and Li (1999) obtained the following expression, which is implicit in $d_{\min}$:

$$1363.3\frac{\sigma^{1.29}\mu_c^{0.02}B^{0.26}}{E^{1.7}\mu_d^{1.02}\rho_c^{0.55}\varepsilon^{0.7}d_{\min}^{2.03}} + 217.3\frac{\sigma^{1.38}B^{0.46}}{E^{0.7}\mu_c\rho_c^{0.84}\varepsilon^{0.89}d_{\min}^{3.11}} = 1 \tag{3}$$

Here, σ is surface tension of water, ε is turbulent kinetic energy dissipation rate per unit mass and ρ and μ are the density and dynamic viscosity, respectively. Subscripts c and d correspond to the continuous (i.e., water) and the dispersed phases (i.e., air), respectively. B is the London–van der Waals constant and is assumed to be equal to 10^{-28} J m and E is the dimensionless curvature radius of the liquid film between two colliding bubbles and is given by

$$E = 12.61 + 2.166\tan^{-1}(2M^{0.8})$$

M is the interface mobility coefficient and is expressed as follows:

$$M = 1.12\frac{\mu_c}{\mu_d}\left(\frac{\pi\sigma}{\rho_c\varepsilon^{2/3}d_{\min}^{5/3}}\right)^{1/2}$$

Although Eq. (3) has not been experimentally verified, Liu and Li (1999) have shown for a case of immobile bubble surface that their numerical predictions agree with the experimental data of Shinnar (1961).

It should be noted that all equations mentioned in this paper are valid for the SI unit system.

3. Experimental

3.1. Flow loop and experimental procedure

A schematic diagram of the experimental loop is shown in Fig. 1. The 35 m long horizontal loop is made of 25.4 mm ID copper tube. A 2.24 kW (3HP) progressive cavity pump [Moyno pump] (P) driven by a variable speed motor is used to circulate water in the loop at a velocity up to 2.9 m/s. A coriolis mass flow meter [Krohne MFM 4085K Corimass, type 300G+] (F) is used to measure mass flow rate, volumetric flow rate and temperature of the flow. A 4 m long double pipe heat exchanger (H) is used to keep the temperature of the loop steady at 18.5 ± 0.5 °C.

The only source of heat generation in the flow is the wall-friction due to the flowing water. This small amount of heat was removed by flowing cold water in the outer pipe when the temperature inside the inner pipe exceeded 19 °C. The flow of cold water was stopped as soon as the temperature reached 18 °C. Two viewing sections (V1 and V2) made of 25.4 mm ID glass tube were placed in the loop. A glass box of rectangular cross-section was fitted over each glass tube. The space between the rectangular box and the tube was filled with water and thus the curvature effect of the tube was removed and undistorted images of bubbles could be obtained.

Bubble size distributions were measured at both viewing sections V1 and V2 when air was injected through injector A1. V1 and V2 are located 0.3 and 27.5 m downstream of the injector A1, respectively. Bubble size distributions were measured only at V2 when injector A2 was used.

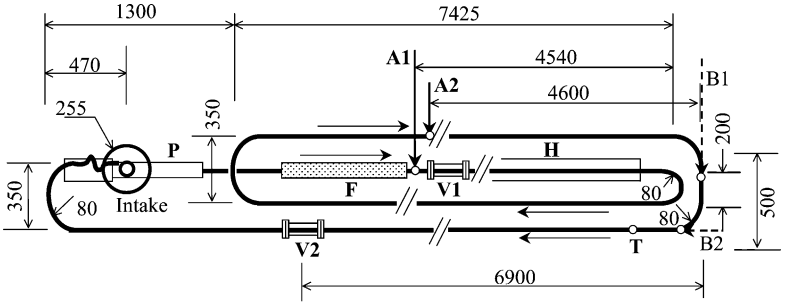

(a) Partial plan view

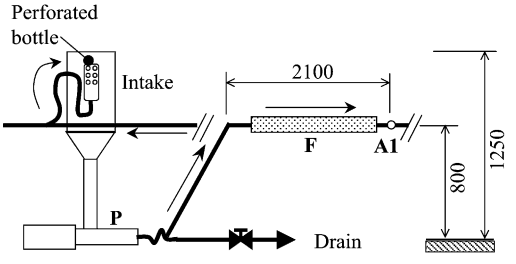

(b) Partial front view

Fig. 1. Schematic diagram of the experimental loop. P—Moyno pump, F—coriolis flow meter, H—heat exchanger, T—thermocouple, A1, A2, B1 and B2—air injection points, V1, V2—viewing sections. Arrows indicate flow direction. Dimensions are in mm.

V2 was located 12 m downstream of the injection point A2. Compressed air was continuously injected through a 2 or 4 mm ID stainless steel tube, which formed a simple T-junction with the loop. The air flowrate was measured with a calibrated rotameter placed in the air supply line. The cross-sectional area of the tank at the inlet of the pump was made large enough to let the air bubbles escape easily to atmosphere. The air–water mixture was discharged vertically upward into the tank. A perforated bottle was attached to the end of the return tube in the tank to prevent bubble entrainment in the flow into the pump suction. It makes the flow into the coriolis mass flow meter free from air bubbles as the air injection points are located further downstream. The average water velocity, U, was thus determined from the recorded volumetric flow rate by dividing it with the pipe cross-sectional area.

3.2. Bubble size measurement

A high-speed CCD camera (MotionScope PCI 1000S) connected to a computer was used to capture images of bubbles at the viewing sections (see Fig. 1). The camera can record 1000 frames per second (fps) and can store 1024 frames in memory. In the present experiments, an imaging rate of 500 fps was used to provide a larger viewing field of 15 mm × 15 mm. The recorded frames were examined and selected carefully so that no bubble was counted more than once. The selected frames were converted into JPEG files to process with image analysis software (SigmaScan Pro 4). From the two-dimensional image (see Fig. 2), SigmaScan Pro measures the area average diameter of the bubble defined by

$$d = \sqrt{\frac{4A}{\pi}} \tag{4}$$

Here, A is the projected area of a bubble in the plane of the two-dimensional image. For each run, approximately 300 bubbles were scanned and the bubble size distribution was obtained. The Sauter mean diameter, d_{32}, was estimated from the raw data:

$$d_{32} = \frac{\sum_{i=1}^{K} n_i d_i^3}{\sum_{i=1}^{K} n_i d_i^2}; \quad \sum_{i=1}^{K} n_i = N \tag{5}$$

where N is bubble count or the total number of bubbles scanned and n_i is the number of bubbles of diameter d_i.

At the magnification used in these experiments, the image processing software has a precision of 0.25 mm. The experiments are repeatable giving the size within 0.5 mm. The average water velocity was kept within ±2.5% of the stated value by adjusting the pump speed. The accuracy of the air–water ratio measurement was ±2%.

For a fixed experimental condition, bubble sizes were evaluated for sampling times of different lengths. The bubble count and the bubble size are listed in Table 1 for average water velocity, U, of 2.9 and 2.1 m/s, air volume fraction, φ, of 0.003 and injector size of 4 mm. In Table 1, $d_{99.8}$ is defined as the diameter of the bubble greater than that of 99.8% of the bubbles in the distribution based on number. It is evident from Table 1 that for a reasonable estimation of the bubble size, the bubble count should be around 300 or more. This criterion was always maintained in processing the data.

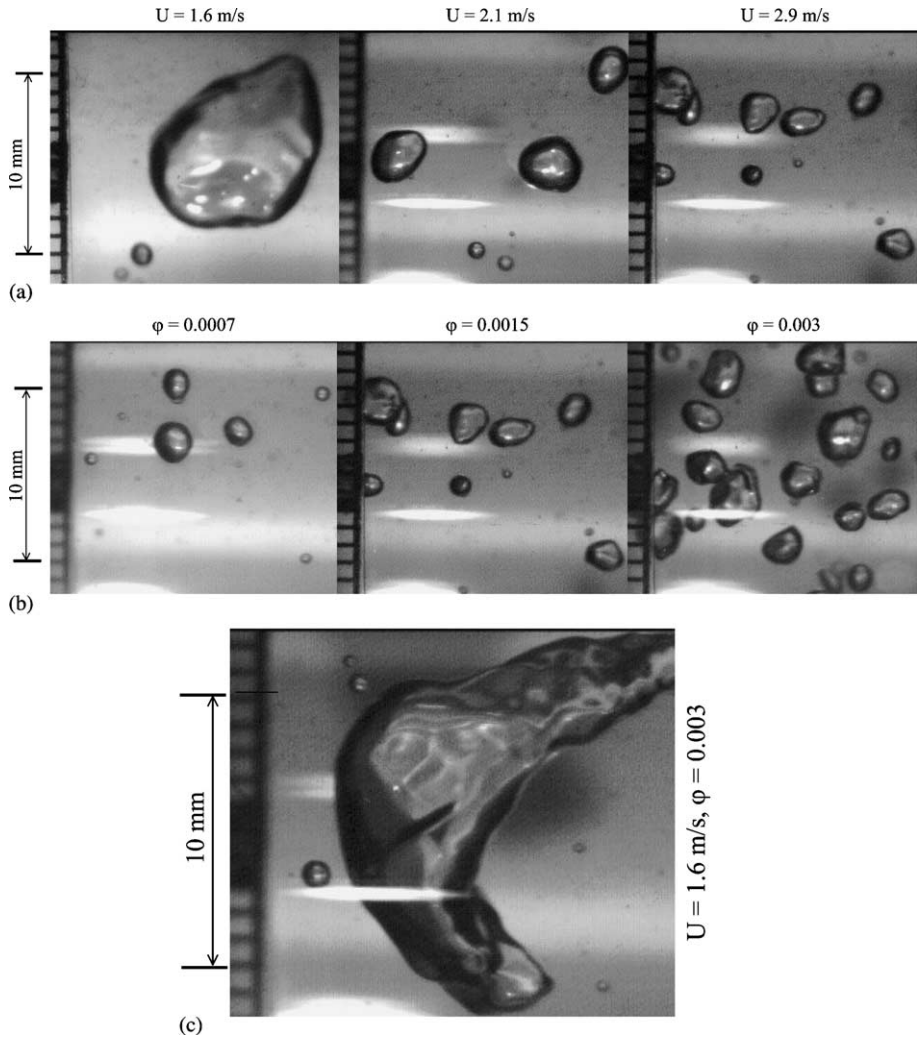

Fig. 2. (a) Effect of average water velocity on bubble size distribution. Images are taken at 27.5 m downstream from the injection point. Injector size is 2 mm and air volume fraction, φ, is 0.0015. (b) Effect of air volume fraction on bubble size distribution. Images are taken at 27.5 m downstream from the injection point. Average water velocity, U, is 2.9 m/s and injector size is 2 mm. (c) Bubble deformation at small velocity of water and large volume fraction of air. Image is taken at 27.5 m downstream. Injector size is 2 mm and air volume fraction, φ, is 0.003.

The results reported in this paper are based on the images taken from the top of each of the viewing sections. It was assumed that each bubble is spherical, so that the diameter measured from the top view is representative of its actual size. To verify this assumption, some images were taken from both the top and the side of the viewing sections at similar conditions. Table 2 shows the comparison of the measured values of $d_{99.8}$ and d_{32} from both positions. It is evident that the difference between the data obtained from the top and those obtained from the side is not significant.

Table 1
Effect of bubble count and sampling time on bubble size measurement

Average water velocity, U, (m/s)	Sampling time (s)	$L = 0.3$ m				$L = 27.5$ m			
		Bubble count, N	Bubble rate (s^{-1})	$d_{99.8} \times 10^3$ (m)	$d_{32} \times 10^3$ (m)	Bubble count, N	Bubble rate (s^{-1})	$d_{99.8} \times 10^3$ (m)	$d_{32} \times 10^3$ (m)
2.9	0.1	150	1500	2.7	1.51	138	1380	5.0	1.86
	0.2	333	1665	3.4	1.52	274	1370	4.2	1.85
	0.4	659	1648	3.4	1.53	534	1335	4.1	1.69
	0.6	1083	1805	3.4	1.53	814	1360	4.1	1.66
	0.8	1374	1718	3.4	1.53	1065	1331	4.1	1.66
	1.0	1761	1761	3.4	1.53	1356	1356	4.1	1.66
2.1	0.1	88	880	7.3	2.29	81	810	5.7	2.95
	0.2	165	825	6.0	2.18	152	760	7.0	2.86
	0.4	328	820	6.8	2.73	274	685	7.1	2.9
	0.6	467	780	6.9	2.9	438	730	7.1	2.9
	0.8	635	794	6.9	2.9	585	732	7.1	2.9
	1.0	811	811	6.9	2.94	752	752	7.1	2.9

Injector size is 4 mm and air volume fraction, φ, is 0.003.

Table 2
Comparison of bubble size measured from top and side of the flow pipe

Average water velocity, U, (m/s)	Bubble count, N		$d_{99.8} \times 10^3$ (m)		$d_{32} \times 10^3$ (m)	
	Top	Side	Top	Side	Top	Side
2.9	357	331	3.4	3.3	1.48	1.48
2.1	336	341	4.8	4.9	2.0	1.94

Injector size is 2 mm, test section length, L is 12 m and air volume fraction, φ, is 0.0015.

Space limitation dictated the use of a couple of bends in the experimental loop to obtain the desired test section length. To quantify the effects of a bend on the measured bubble size, initially some tests were performed with two additional air injectors B1 and B2. The corresponding measured bubble sizes using the two injectors were found to be within 0.1 mm, which is of the order of the experimental error.

4. Results and discussion

Experiments were performed to determine bubble size distributions for three average water velocities ($U = 1.6$, 2.1 and 2.9 m/s) for each of the three test sections (test section length, $L = 0.3$, 12 and 27.5 m). Three air volume fractions ($\varphi = 0.0007$, 0.0015 and 0.0030) and two air injectors of 2 and 4 mm ID were used. Effects of average water velocity and air volume fraction on bubble size distribution are clearly visible in Fig. 2a and b, respectively. Fig. 2c shows the deformation of

a bubble at $U = 1.6$ m/s and $\varphi = 0.003$. At large air volume fractions and small water velocities, the bubbles become highly deformed. No experiment was conducted at this condition.

4.1. Bubble size distribution

The distributions of cumulative number percentage undersize of bubbles are shown in Fig. 3 for the 2 mm injector and air volume fraction, φ, of 0.0015. The cumulative distributions are plotted using log-probability scales. Beyond $d = 0.5$ mm, the symbols almost follow straight lines in all cases, implying that the bubble size distributions generally follow a log-normal pattern. The log-normal distribution function in number, $f(d)$, is expressed as follows:

$$f(d) = \frac{\partial \Phi}{\partial \ln d} = \frac{1}{\sqrt{2\pi}\ln \sigma_g} \exp\left[-\frac{1}{2}\left(\frac{\ln(d/d_g)}{\ln \sigma_g} \right)^2 \right] \tag{6}$$

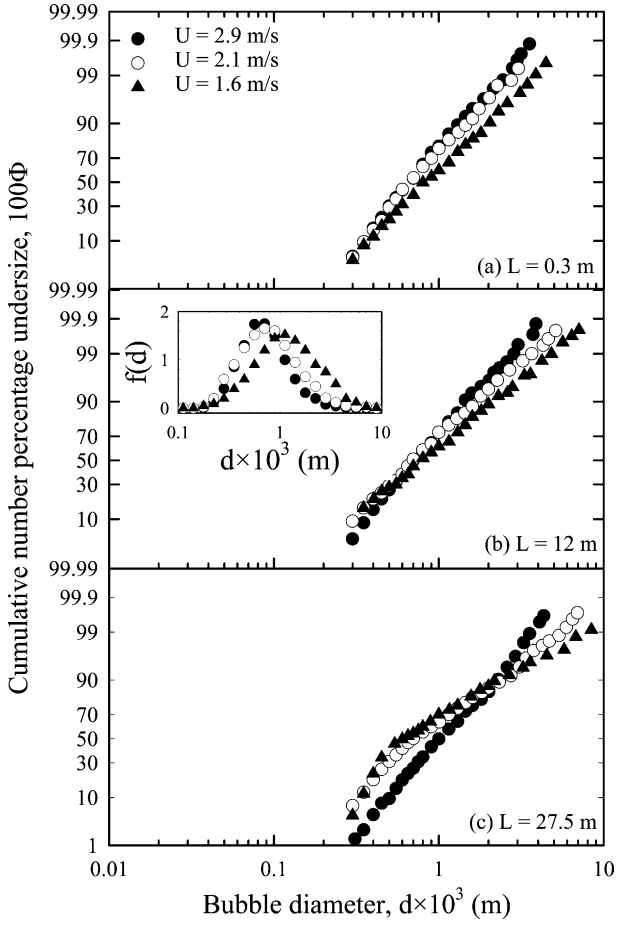

Fig. 3. Cumulative distribution of bubble size for different average water velocities. Injector size is 2 mm and air volume fraction, φ, is 0.0015 (corresponding distribution density function $f(d)$ for case b is shown in the inset).

Here, Φ gives the cumulative number fraction of bubbles having diameters smaller than a given diameter, d. The geometric mean size, d_g, and the geometric mean standard deviation, σ_g, are estimated from the raw data as follows:

$$d_g = \sqrt[K]{\prod_{i=1}^{K} (d_i)^{n_i}} \tag{7}$$

$$\ln \sigma_g = \sqrt{\frac{\sum_{i=1}^{K} n_i (\ln d_i - \ln d_g)^2}{N}} \tag{8}$$

In Fig. 3, one can observe that the bubble size distribution becomes wider with decreasing average water velocity and increasing test section length. Near the inlet section ($L = 0.3$ m), the largest bubble observed is approximately 3.6 mm in diameter at $U = 2.9$ m/s and 6.1 mm in diameter at $U = 1.6$ m/s. At $L = 12$ m, the largest bubbles are roughly 3.7 mm in diameter at $U = 2.9$ m/s and 8.5 mm in diameter at $U = 1.6$ m/s. At $L = 27.5$ m, the bubbles became larger and the largest bubbles are approximately 4.9 mm in diameter at $U = 2.9$ m/s and 11.6 mm in diameter at $U = 1.6$ m/s. As soon as introduced into the pipe, the air becomes exposed to a destabilizing energy due to the turbulent velocity fluctuations in the flow. As a result, the continuous air-jet breaks into bubbles. This energy, ε, is a strong function of the water velocity as $\varepsilon \sim U^3/D$. At larger velocities, the flow possesses more energy and the continuous air-jet is broken into smaller bubbles with a narrower size distribution. On the other hand, at smaller velocities, relatively large bubbles can survive due to the smaller energy of the flow and a wider size distribution is obtained.

As the bubbles traverse along the pipe, they interact with the turbulent eddies and among themselves. The large bubbles break up and the small bubbles coalesce. Since the bubble size distribution becomes wider and skews towards a larger diameter at the downstream locations, the coalescence process dominates in the present experiments.

For the case of $U = 2.9$ m/s, Fig. 4a shows that at $L = 12$ and 27.5 m, the entire cumulative distribution curve shifted to the right, which is caused by coalescence of bubbles. However, at the smaller velocity of 1.6 m/s, as shown in Fig. 4b, the upper portion of the curve is shifted to the right whereas the lower portion is shifted to the left, which progressively increases the width of the distribution with increasing pipe length. This behavior may be attributed to an increase in the number percentage of small bubbles. Generation of small bubbles through the breakup mechanism may raise their number percentage and elevate the distribution curve at the lower end. On the other hand, a portion of the smaller bubbles could coalesce together to form a few larger bubbles resulting in an increase in the number percentage of the remaining smaller bubbles. To evaluate the relative importance of these two (breakup and coalescence) mechanisms, the number of bubbles passing through each viewing section per second is examined. Fig. 5 shows that the number rate of bubbles passing through the viewing sections decreases with increasing pipe length and decreasing average water velocity. This behavior confirms that coalescence is the dominant mechanism for all water velocities of the present study. The decrease of the normalized local bubble rate is larger at smaller average water velocities, which implies that coalescence becomes even more dominant as the average water velocity decreases.

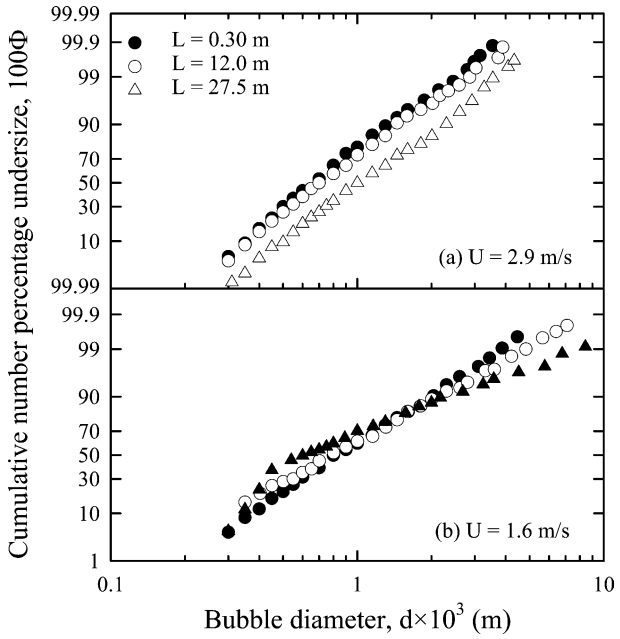

Fig. 4. Bubble size distribution for different pipe lengths when (a) $U = 2.9$ m/s and (b) $U = 1.6$ m/s. Injector size is 2 mm and air volume fraction, φ, is 0.0015.

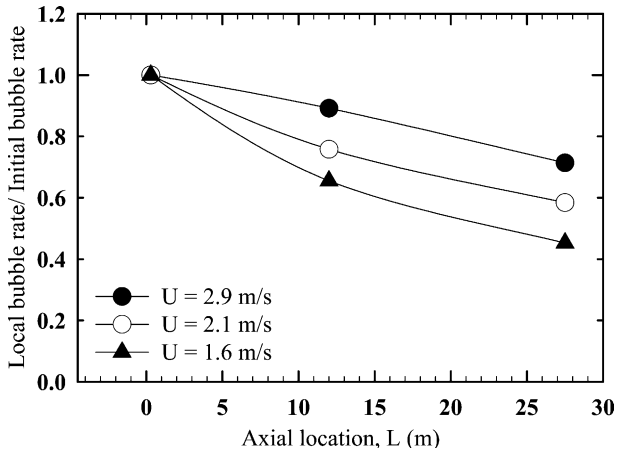

Fig. 5. Number rate of bubbles passing through different axial locations. Injector size is 2 mm and air volume fraction, φ, is 0.0015. Lines are trend lines only.

Martinez-Bazan et al. (2000) have shown that at stable conditions (i.e. invariant with pipe length), the distribution curves collapse to a single curve when the diameters are scaled by d_{32}. This implies a constant width of the distribution for all cases. Hesketh et al. (1987) also speculated that a constant value of 1.3 could be assigned for the standard deviation (a measure of the width of the distribution), when the distribution is invariant with pipe length in a 25.4 mm ID horizontal

pipe. The cumulative distributions of d/d_{32} for all of the experimental runs discussed above are shown in Fig. 6 using a log-probability scale. Fig. 6a shows that at 2.9 m/s, the curves for the three test section lengths collapse on each other, indicating that in this case the distributions likely attained a condition that is invariant with pipe length. The standard deviation, σ_g for the three distributions in Fig. 6a can be found in Table 3 and is close to 1.7. For other cases shown in Fig. 6b and c, however, the distributions do not collapse on each other and thus are not invariant with pipe length. In these cases, the standard deviation of bubble diameters is as large as 2. Most likely, the distributions at smaller velocities would become invariant with pipe length if the test section were longer, because this would allow more time for small bubbles to coalesce.

It is evident from Fig. 6 that the distribution curves for d/d_{32} intersect at 99.8% and a unique value for $d_{99.8}/d_{32} = 2.2$ is obtained. The values reported by other experimenters are in the range of 1.67 (Steinmeyer, 1995) to 3.33 (Calabrese et al., 1986a) for different systems. Based on log-normal distribution, one can show that

$$\frac{d_{99.8}}{d_{32}} = \exp\left[-(2.5\ln^2\sigma_g - 2.88\ln\sigma_g)\right] \tag{9}$$

The ratio $d_{99.8}/d_{32}$ is a weak function of the standard deviation, σ_g, and thus not significantly affected by variation of σ_g. Knowledge of $d_{99.8}$ can, therefore, provide the corresponding value of the Sauter mean diameter d_{32}, which is very useful as a design parameter. Moreover, with the knowledge of the standard deviation, σ_g, it is possible to quantify the size distribution through $d_{99.8}$.

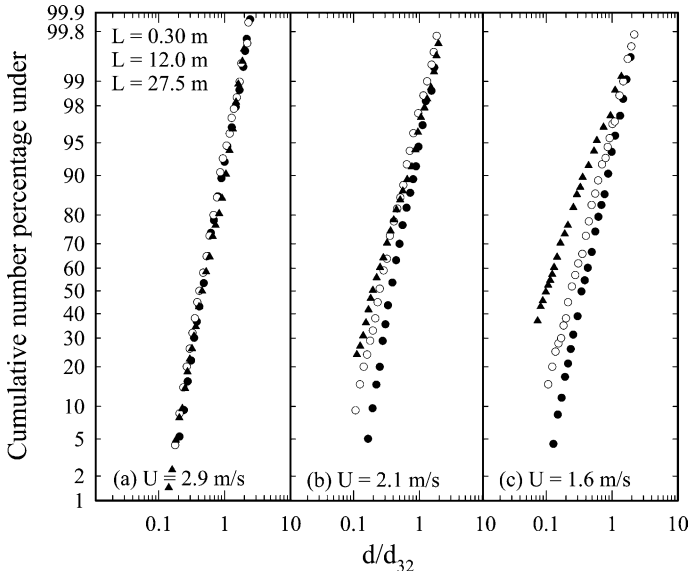

Fig. 6. Cumulative distribution of d/d_{32} for different pipe lengths when (a) $U = 2.9$ m/s, (b) $U = 2.1$ m/s and (c) $U = 1.6$ m/s. Injector size is 2 mm and air volume fraction, φ, is 0.0015.

Table 3
Bubble size and distribution parameters

Average water velocity, U, (m/s)	Bubble count, N	Observed largest bubble dia. $\times 10^3$ (m)	$d_{99} \times 10^3$ (m)	$d_{99.8} \times 10^3$ (m)	$d_{32} \times 10^3$ (m)	d_{32}/d_{99}	$d_{32}/d_{99.8}$	Mean $d_g \times 10^3$ (m)	Std. dev., σ_g
$L = 0.3$ m									
2.9	775	3.58	2.4	3.3	1.45	0.60	0.44	0.67	1.67
2.1	456	4.31	3.0	4.1	1.80	0.60	0.44	0.7	1.72
1.6	424	6.11	4.0	5.5	2.33	0.58	0.42	0.85	1.80
$L = 12$ m									
2.9	691	3.7	2.5	3.4	1.48	0.59	0.44	0.7	1.7
2.7	850	3.33	2.6	3.6	1.61	0.62	0.45	0.75	1.73
2.3	300	3.8	3.0	4.1	1.71	0.57	0.42	0.78	1.73
2.1	464	5.5	4.0	5.0	2.06	0.52	0.41	0.75	1.80
1.8	1152	5.7	4.5	5.4	2.23	0.50	0.41	0.80	1.83
1.6	905	8.5	5.5	7.5	3.26	0.59	0.43	0.82	1.90
1.3	656	8.9	6.2	9.0	3.41	0.55	0.38	0.85	1.91
$L = 27.5$ m									
2.9	553	4.92	3.7	4.50	2.12	0.57	0.47	1.03	1.79
2.1	666	8.5	5.8	8.0	3.56	0.61	0.44	0.8	1.9
1.6	240	11.65	9.5	12.0	6.0	0.63	0.50	0.75	2.01

Injector size is 2 mm and air volume fraction, φ, is 0.0015.

4.2. Maximum bubble size

It is evident from Table 3 that in the present experiments, $d_{99.8}$ is also close to the experimentally observed largest bubble diameter. Therefore, $d_{99.8}$ is a good choice to represent the maximum bubble size and this section will focus on its estimation. Fig. 7a shows the variation of diameter $d_{99.8}$ as a function of the superficial water velocity, U, for different axial distances downstream of the injector. In these experiments, 0.15% air ($\varphi = 0.0015$) was injected using the 2 mm injector. The solid line shows the maximum bubble diameter d_{max} obtained from Eq. (2). This is the maximum bubble size that is not expected to break up under the given flow conditions. The broken line in Fig. 7a represents the minimum bubble diameter, d_{min}, calculated from Eq. (3), which is predicted to be stable against coalescence. Fig. 7a illustrates that the present experiments were conducted in the coalescence dominant regime, where d_{max} is greater than d_{min}. In this regime, bubbles may undergo breakup or coalescence depending on their size and residence time in the pipeline.

When the predicted d_{min} is greater than the predicted d_{max}, which occurs at much average larger water velocities than those studied here, the breakup process is dominant. In this regime, known as the breakup dominant regime, Eq. (3) is not applicable (Thomas, 1981). However, the concept of maximum bubble diameter is linked to the breakup theory and experimental $d_{99.8}$ will be comparable to the prediction of Eq. (2) irrespective of the dominance of either breakage or coalescence.

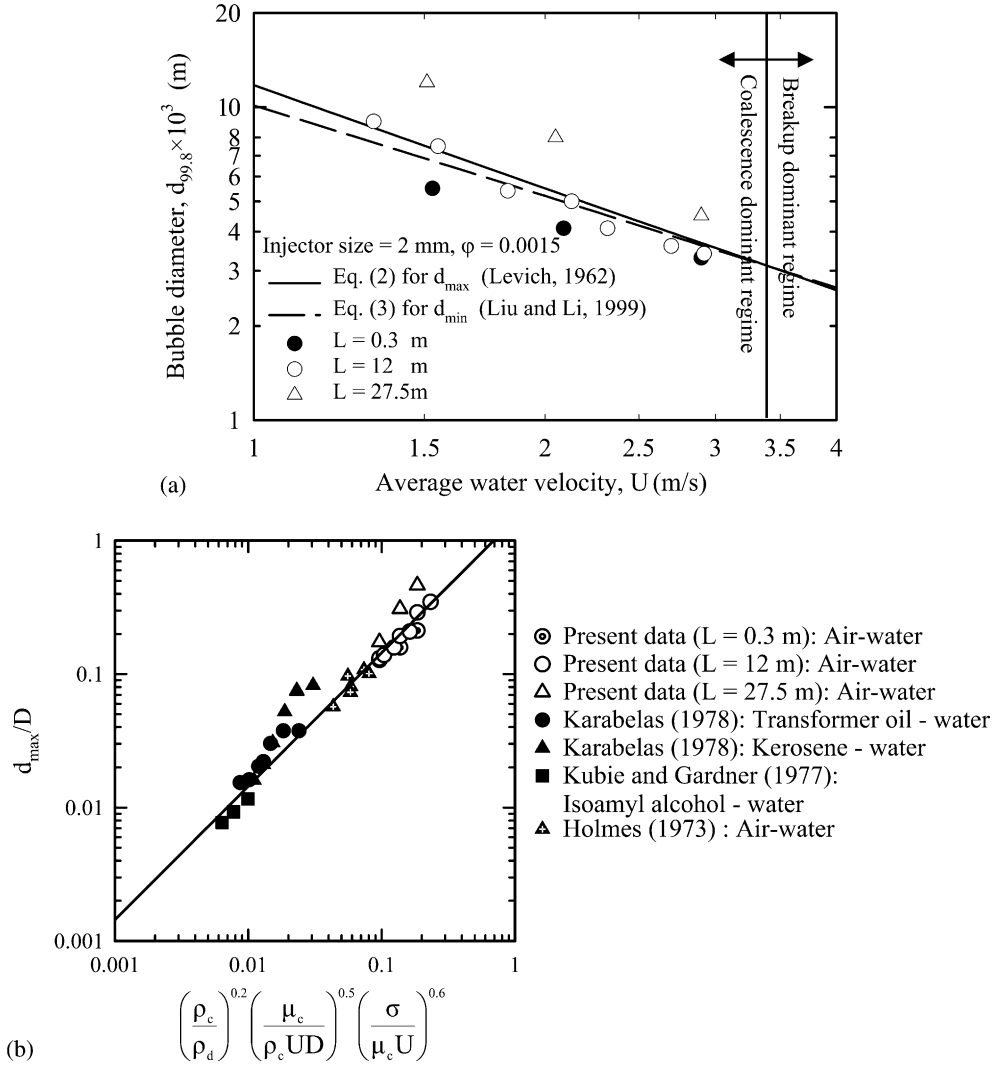

Fig. 7. (a) Effect of average water velocity and pipe length on maximum bubble diameter, $d_{99.8}$. (b) Comparison of present data with data of other studies. The solid line represents Levich's (1962) theory.

The solid symbols in Fig. 7a indicate bubble diameters, $d_{99.8}$, measured at the inlet ($L = 0.3$ m). For small average water velocities, the bubbles are considerably smaller than the corresponding d_{min} and hence, have a high potential to coalesce. They continue to coalesce with increasing length, resulting in largest bubble diameters (open triangles in Fig. 7a) well above the corresponding d_{max} at $L = 27.5$ m. The predicted d_{max} is smaller than the experimentally determined $d_{99.8}$ because Eq. (2) was established by considering only the breakage of a solitary bubble. Eq. (2) does not account for interactions with other bubbles or the influence of coalescence on d_{max}. As the average water velocity increases, the influence of coalescence diminishes (see Fig. 5) and the system approaches the breakup dominant regime. Thus for $U = 2.9$ m/s, the maximum bubble diameter, d_{max}, predicted by Eq. (2) is close to the experimentally determined value of $d_{99.8}$.

Data presented in Fig. 7a are replotted in Fig. 7b along with some data from the studies of Holmes (1973), Kubie and Gardner (1977) and Karabelas (1978). Eq. (2) is rearranged in non-dimensional form, Eq. (10), to generalize it for different two-phase fluid systems and operating conditions. All notations in Eq. (10) are defined in connection with Eq. (2).

$$\frac{d_{\max}}{D} = 1.38(We_c)^{0.6}\left(\frac{\rho_c}{\rho_d}\right)^{0.2}\left(\frac{\mu_c}{\rho_c UD}\right)^{0.5}\left(\frac{\sigma}{\mu_c U}\right)^{0.6} \tag{10}$$

The solid line in Fig. 7b represents Eq. (10) with $We_c = 1.1$. The data are most scattered on the upper side of the curve. They are from both this study and Karabelas' (1978) kerosene–water

Table 4
Effect of air volume fraction on bubble size and distribution when U is 2.9 m/s (panel A) and U is 2.1 m/s (panel B) and injector size is 2 mm

Air volume fraction, φ	Bubble count, N	Observed largest bubble dia. $\times 10^3$ (m)	$d_{99} \times 10^3$ (m)	$d_{99.8} \times 10^3$ (m)	$d_{32} \times 10^3$ (m)	d_{32}/d_{99}	$d_{32}/d_{99.8}$	Mean $d_g \times 10^3$ (m)	Std. dev., σ_g
Panel A									
$L = 0.3$ m									
0.0007	688	3.69	2.3	3.1	1.38	0.6	0.44	0.72	1.66
0.0015	775	3.58	2.4	3.3	1.45	0.60	0.44	0.67	1.67
0.003	634	4.62	2.8	3.7	1.68	0.6	0.45	0.82	1.68
$L = 12$ m									
0.0007	521	2.78	2.2	2.9	1.3	0.59	0.45	0.63	1.64
0.0015	691	3.7	2.5	3.4	1.48	0.59	0.44	0.7	1.7
0.003	750	5.15	3.3	4.7	2.02	0.61	0.43	0.81	1.78
$L = 27.5$ m									
0.0007	575	3.54	2.7	3.5	1.55	0.57	0.44	0.76	1.7
0.0015	553	4.92	3.7	4.5	2.12	0.57	0.47	1.03	1.79
0.003	777	5.7	4.2	6.0	2.4	0.57	0.40	1.27	1.84
Panel B									
$L = 0.3$ m									
0.0007	375	3.22	2.2	3.0	1.4	0.64	0.46	0.61	1.66
0.0015	456	4.31	3.0	4.1	1.8	0.6	0.44	0.7	1.72
0.003	371	5.7	4.0	5.6	2.4	0.6	0.43	0.88	1.9
$L = 12$ m									
0.0007	848	5.0	3.1	4.2	1.9	0.61	0.45	0.61	1.76
0.0015	464	5.5	4.0	5.0	2.06	0.52	0.41	0.75	1.8
0.003	295	7.08	4.8	7.0	3.2	0.66	0.44	0.78	2.0
$L = 27.5$ m									
0.0007	655	8.07	4.8	7.1	3.25	0.67	0.45	0.67	1.8
0.0015	666	8.5	5.8	8.0	3.56	0.61	0.44	0.8	1.9
0.003	290	11.51	7.5	11	4.8	0.64	0.44	0.9	2.1

experiments. It implies that some of those experiments were probably conducted in the coalescence dominant regime.

A bubble of diameter greater than d_{max} may survive in spite of breakage due to the influence of coalescence, which, in turn, depends on the air volume fraction. Holmes (1973) used only 0.1% air, whereas Andreussi et al. (1999) used 20% air in experiments in the breakup dominant regime. The data of Andreussi et al. (1999) exhibited no influence of air volume fraction on coalescence and, hence, on bubble size up to 3% air by volume. In the coalescence dominant regime, on the other hand, the influence of air volume fraction on bubble size was studied by Calderbank (1958). His experiments in stirred tanks showed a significant dependence of bubble Sauter mean diameter, d_{32}, on the air volume fraction, φ, as follows:

$$d_{32} \propto \sqrt{\varphi} + c \tag{11}$$

where c is a constant for a given set of fluid and system properties.

In the present study, the air volume fraction, φ, was varied from 0.0007 to 0.006 (see Tables 4 and 5). Figs. 8 and 9 show the effect of air volume fraction on the bubble size distribution at $U = 2.9$ and 2.1 m/s, respectively. It is clear that the higher the air volume fraction is, the more the

Table 5
Effect of air volume fraction on bubble size and distribution when U is 2.9 m/s (panel A) and U is 2.1 m/s (panel B) and injector size is 4 mm

Air volume fraction, φ	Bubble count, N	Observed largest bubble dia. $\times 10^3$ (m)	$d_{99} \times 10^3$ (m)	$d_{99.8} \times 10^3$ (m)	$d_{32} \times 10^3$ (m)	d_{32}/d_{99}	$d_{32}/d_{99.8}$	Mean $d_g \times 10^3$ (m)	Std. dev., σ_g
Panel A									
$L = 0.3$ m									
0.0015	778	4.04	2.4	3.2	1.46	0.60	0.45	0.68	1.58
0.003	1761	4.29	2.7	3.4	1.53	0.57	0.45	0.75	1.57
0.035	705	4.36	3.3	4.5	1.93	0.58	0.43	0.76	1.71
$L = 27.5$ m									
0.0015	503	3.05	2.7	3.5	1.55	0.57	0.44	0.93	1.62
0.003	1356	3.7	2.7	3.6	1.64	0.61	0.46	0.91	1.64
0.035	411	3.67	4.0	5.5	1.99	0.50	0.36	1.18	1.75
Panel B									
$L = 0.3$ m									
0.0015	504	4.7	3.0	4.4	1.85	0.61	0.42	0.60	1.80
0.003	811	6.9	4.8	6.9	2.94	0.61	0.42	0.78	1.95
0.06	792	9.07	5.8	8.5	3.72	0.64	0.44	0.97	2.02
$L = 27.5$ m									
0.0015	333	5.7	3.9	5.5	2.27	0.58	0.41	0.90	1.85
0.003	752	6.35	5.0	7.1	2.9	0.58	0.41	1.13	1.9
0.06	361	8.79	6.5	9.0	3.84	0.59	0.42	1.76	2.11

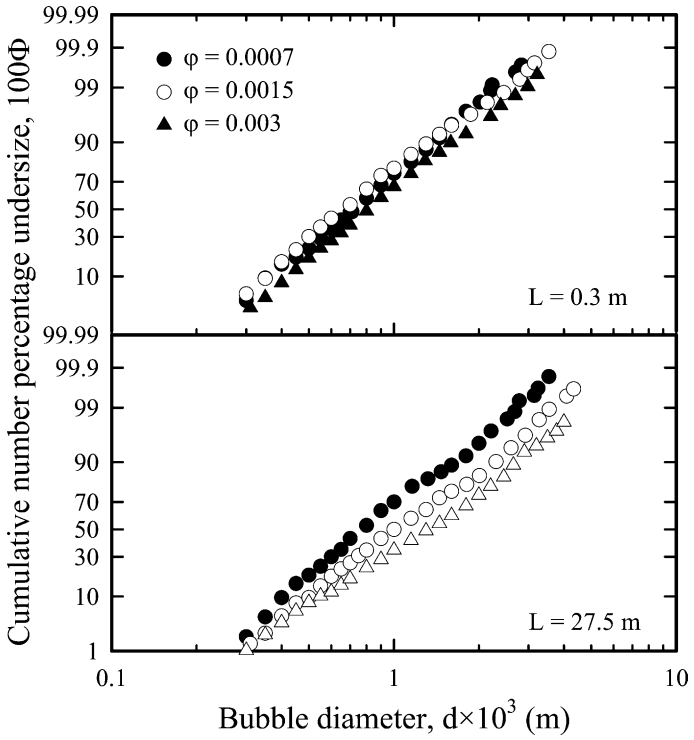

Fig. 8. Effect of air volume fraction on bubble size distribution. Average water velocity, U, is 2.9 m/s and injector size is 2 mm.

distribution curves shift towards the right due to coalescence, thereby resulting in larger values of $d_{99.8}$. The effect of air volume fraction on bubble size is shown in Fig. 10a and b and Table 4. At both $U = 2.9$ and $U = 2.1$ m/s, $d_{99.8}$ increases with air volume fraction as well as with distance from the injection point. At 2.1 m/s, which is well inside the coalescence dominant regime, the bubble size increases considerably with pipe length even for $\varphi = 0.0007$. However, at $U = 2.9$ m/s, which is close to the breakup dominant regime, the bubble size is more stable for $\varphi = 0.0007$ and 0.0015 and is close to the predictions of Eq. (2) due to Levich (1962).

In an attempt to obtain large bubbles at the inlet to reduce the probability of coalescence, some experiments were performed with a 4 mm injector for air volume fractions, $\varphi = 0.0015$, 0.003 and 0.035. The size analysis results are given in Table 5. In this case, a significantly large number of small bubbles was observed along with a few large bubbles. The large bubbles are less prone to coalescence and most of the available energy is used up by coalescence of small bubbles. Hence, unlike the results of the tests conducted with the 2 mm injector, $d_{99.8}$ did not increase appreciably at the downstream locations. Fig. 11 shows that with the 4 mm injector and $U = 2.9$ m/s, the experimental $d_{99.8}$ values agree well with the predictions of Eq. (2) for both air volume fractions, $\varphi = 0.0015$ and 0.003. The agreement is poor for $\varphi = 0.035$. One can thus conclude that in these experiments, where coalescence is dominant, Levich's (1962) theory is useful for predicting the maximum bubble diameter, $d_{99.8}$, for very small air volume fractions. Also, the injector size

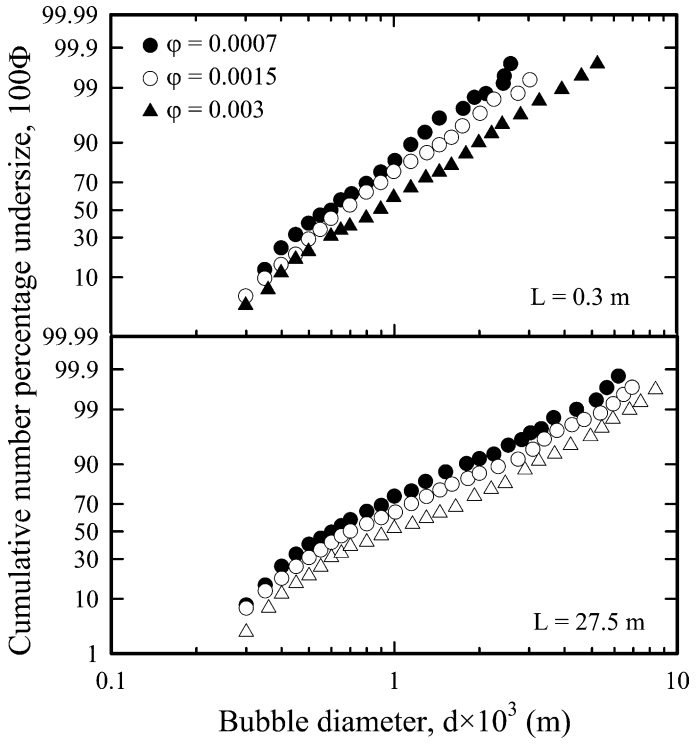

Fig. 9. Effect of air volume fraction on bubble size distribution. Average water velocity, U, is 2.1 m/s and injector size is 2 mm.

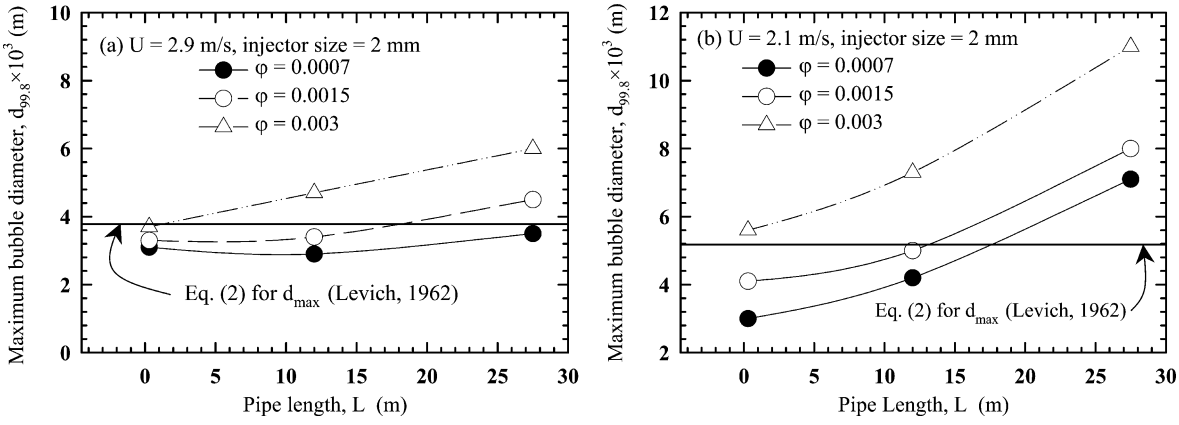

Fig. 10. Effect of air volume fraction and pipe length on maximum bubble diameter, $d_{99.8}$, when (a) 2.9 m/s and (b) 2.1 m/s. Injector size is 2 mm. Lines are trend lines only.

influences the development of bubble size distribution due to its contribution in generating the inlet bubble size distribution.

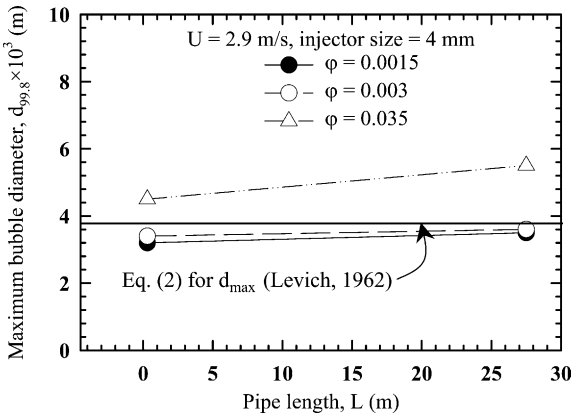

Fig. 11. Effect of air volume fraction and pipe length on maximum bubble diameter, $d_{99.8}$, when U is 2.9 m/s and injector size is 4 mm. Lines are trend lines only.

5. Conclusions

This study improves the current understanding of the evolution of bubble size and distribution during the coalescence dominant turbulent flow of an air–water system. It is known from previous studies that bubble size distributions in turbulent pipe flow in the breakup dominant regime follow a log-normal pattern. The present study shows that the log-normal bubble size distribution is also valid for coalescence dominant turbulent pipe flow. A continuous stream of air entering laterally into a flowing stream of water generates bubbles having a log-normal size distribution. As the bubbles traverse downstream, they increase in size due to coalescence. At larger average water velocities, the log-normal pattern of the bubble size distribution is maintained downstream of the injection point. At smaller average water velocities, the distribution deviates slightly at both ends (large and small) from the log-normal pattern.

The air bubble size distributions measured during this study are characterized by a constant value of the ratio $d_{99.8}/d_{32}$, which is about 2.2 (i.e., $d_{32}/d_{99.8} = 0.45$). This ratio is nearly independent of average water velocity, pipe length, air volume fraction and air injector diameter. The distributions of d/d_{32} are also invariant with pipe length at $U = 2.9$ m/s and the standard deviation of the bubble size for this condition is roughly 1.7. For small water velocities, the distributions of d/d_{32} are not invariant with pipe length and the standard deviation of the bubble size is as large as 2.

To predict the distribution of bubble sizes, it is proposed to use $d_{99.8}$ as the characteristic maximum bubble diameter. The maximum bubble size may be estimated from Levich's (1962) breakup theory, Eq. (2), for small air volume fractions.

The air volume fraction significantly affects the bubble size. However, its effect is reduced as the velocity of water is increased. The injector size has only a secondary effect on the development of bubble size distribution through its role in generating the initial bubbles.

At $U = 2.9$ m/s, it is found that the prediction of $d_{\max}$ through Levich's (1962) breakup theory agrees with the $d_{99.8}$ values for air volume fractions up to 0.0015 with a 2 mm injector and up to 0.003 with a 4 mm injector. In other cases, $d_{99.8}$ increases monotonically with pipe length.

Acknowledgements

The authors gratefully acknowledge the financial support from the Natural Sciences and Engineering Research Council of Canada (NSERC) and Syncrude Canada Ltd. for this project.

References

Andreussi, P., Paglianti, A., Silva, F., 1999. Dispersed bubble flow in horizontal pipes. Chem. Eng. Sci. 54, 1101–1107.
Angeli, P., 2001. Droplet size in two-phase liquid dispersed pipeline flows. Chem. Eng. Technol. 24, 431–434.
Angeli, P., Hewitt, G.F., 2000. Drop size distributions in horizontal oil–water dispersed flows. Chem. Eng. Sci. 55, 3133–3143.
Calabrese, R.V., Chang, T.P.K., Dang, P.T., 1986a. Drop breakup in turbulent stirred-tank contactors. Part I: Effect of dispersed phase viscosity. AIChE J. 32, 657–666.
Calabrese, R.V., Wang, C.Y., Bryner, N.P., 1986b. Drop breakup in turbulent stirred-tank contactors. Part III: Correlations for mean size and drop size distribution. AIChE J. 32, 677–681.
Calderbank, P.H., 1958. Physical rate processing in industrial fermentation. Part I: The interfacial area in gas–liquid contacting with mechanical agitation. Trans. IChemE 36, 443–463.
Chesters, A.K., 1991. The modelling of coalescence processes in fluid–liquid dispersions: A review of current understanding. Trans. IChemE 69 (Part A), 259–270.
Church, J.M., Shinnar, R., 1961. Stabilizing liquid–liquid dispersions by agitation. Ind. Eng. Chem. 53, 479–484.
Collins, S.B., Knudsen, J.G., 1970. Drop-size distributions produced by turbulent pipe flow of immiscible liquids. AIChE J. 16, 1072–1080.
Davies, J.T., 1987. A physical interpretation of drop sizes in homogenizers and agitated tanks, including the dispersion of viscous oils. Chem. Eng. Sci. 42, 1671–1676.
Hesketh, R.P., Russell, T.W.F., Etchells, A.W., 1987. Bubble size in horizontal pipelines. AIChE J. 33, 663–667.
Hesketh, R.P., Etchells, A.W., Russell, T.W.F., 1991a. Experimental observations of bubble breakage in turbulent flow. Ind. Eng. Chem. Res. 30 (5), 835–841.
Hesketh, R.P., Etchells, A.W., Russell, T.W.F., 1991b. Bubble breakage in pipeline flow. Chem. Eng. Sci. 46, 1–9.
Hinze, J.O., 1955. Fundamentals of the hydrodynamic mechanism of splitting in dispersion processes. AIChE J. 1, 289–295.
Holmes, T.L., 1973. Fluid mechanics of horizontal bubble flow. Ph.D. Thesis, University of Delaware.
Karabelas, A.J., 1978. Droplet size spectra generated in turbulent pipe flow of dilute liquid/liquid dispersions. AIChE J. 24, 170–180.
Kolmogoroff, A.N., 1949. On the breaking of drops in turbulent flow. Dokl. Akad. Nauk. SSSR 66, 825–828.
Kostoglou, M., Karabelas, A.J., 1998. On the attainment of steady state in turbulent pipe flow of dilute dispersions. Chem. Eng. Sci. 53, 505–513.
Kubie, J., Gardner, G.C., 1977. Drop sizes and drop dispersion in straight horizontal tubes and in helical coils. Chem. Eng. Sci. 32, 195–202.
Levich, V.G., 1962. Physiochemical Hydrodynamics. Prentice Hall, Englewood Cliffs, NJ. p. 464.
Liu, S., Li, D., 1999. Drop coalescence in turbulent dispersions. Chem. Eng. Sci. 54, 5667–5675.
Martinez-Bazan, C., Montanes, J.L., Lasheras, J.C., 1999a. On the breakup of an air bubble injected into a fully developed turbulent flow. Part 1. Breakup frequency. J. Fluid Mech. 401, 157–182.
Martinez-Bazan, C., Montanes, J.L., Lasheras, J.C., 1999b. On the breakup of an air bubble injected into a fully developed turbulent flow. Part 2. Size PDF of the resulting daughter bubbles. J. Fluid Mech. 401, 183–207.
Martinez-Bazan, C., Montanes, J.L., Lasheras, J.C., 2000. Bubble size distribution resulting from the breakup of an air cavity injected into a turbulent water jet. J. Phys. Fluids 12, 145–148.
Parthasarathy, R., Jameson, G.J., Ahmed, N., 1991. Bubble breakup in stirred vessels-prediction of the Sauter mean diameter. Trans. IChemE 69 (Part A), 295–301.
Risso, F., 2000. The mechanisms of deformation and breakup of drops and bubbles. Multiphase Sci. Technol. 12, 1–50.

Sevik, M., Park, S.H., 1973. The splitting of drops and bubbles by turbulent fluid flow. J. Fluids Eng. 95, 53–60.
Shinnar, R., 1961. On the behaviour of liquid dispersions in mixing vessels. J. Fluid Mech. 10, 259–275.
Shinnar, R., Church, J.M., 1960. Predicting particle size in agitated dispersions. Ind. Eng. Chem. 52, 253–256.
Simmons, M.J.H., Azzopardi, B.J., 2001. Drop size distributions in dispersed liquid–liquid pipe flow. Int. J. Multiphase Flow 27, 843–859.
Steinmeyer, D., 1995. Use power/mass to estimate drop size in gas/liquid contactors. Chem. Eng. Prog., 72–80.
Swartz, J.E., Kessler, D.P., 1970. Single drop breakup in developing turbulent pipe flow. AIChE J. 16, 254–260.
Thomas, R.M., 1981. Bubble coalescence in turbulent flows. Int. J. Multiphase Flow 7, 709–717.
Tsouris, C., Tavlarides, L.L., 1994. Breakage and coalescence models for drops in turbulent dispersions. AIChE J. 40, 395–406.
Walter, J.F., Blanch, H.W., 1986. Bubble break-up in gas–liquid bioreactors: break-up in turbulent flows. Chem. Eng. J. 32, B7–B17.
Ward, J.P., Knudsen, J.G., 1967. Turbulent flow of unstable liquid–liquid dispersions: drop sizes and velocity distributions. AIChE J. 13, 356–365.
Wilkinson, P.M., Van Schayk, A., Spronken, J.P.M., Van Dierendonck, L.L., 1993. The influence of gas density and liquid properties on bubble breakup. Chem. Eng. Sci. 48, 1213–1226.